

See discussions, stats, and author profiles for this publication at: <https://www.researchgate.net/publication/280571400>

# A Balanced Face-On to Edge-On Texture Ratio in Naphthalene Diimide-Based Polymers with Hybrid Siloxane Chains Directs Highly Efficient Electron Transport

ARTICLE *in* MACROMOLECULES · JULY 2015

Impact Factor: 5.8 · DOI: 10.1021/acs.macromol.5b01012

---

READS

79

## 8 AUTHORS, INCLUDING:



[Yiho Kim](#)

Ulsan National Institute of Science and Tech...

6 PUBLICATIONS 242 CITATIONS

[SEE PROFILE](#)



[Junghoon Lee](#)

University of California, Santa Barbara

23 PUBLICATIONS 609 CITATIONS

[SEE PROFILE](#)



[Tae Joo Shin](#)

Ulsan National Institute of Science and Tech...

127 PUBLICATIONS 2,586 CITATIONS

[SEE PROFILE](#)



[Kyung-Wan Nam](#)

Dongguk University

98 PUBLICATIONS 2,344 CITATIONS

[SEE PROFILE](#)

## A Balanced Face-On to Edge-On Texture Ratio in Naphthalene Diimide-Based Polymers with Hybrid Siloxane Chains Directs Highly Efficient Electron Transport

Yiho Kim,<sup>†</sup> Dang Xuan Long,<sup>‡</sup> Junghoon Lee,<sup>†</sup> Gyoongsik Kim,<sup>†</sup> Tae Joo Shin,<sup>§</sup> Kyung-Wan Nam,<sup>‡</sup> Yong-Young Noh,<sup>\*‡</sup> and Changduk Yang<sup>\*†</sup>

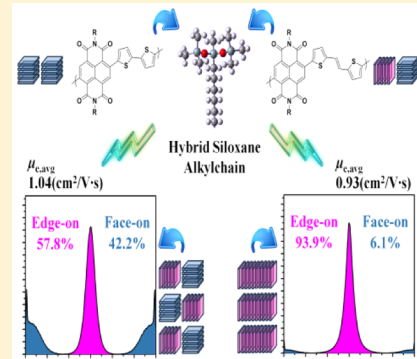
<sup>†</sup>School of Energy and Chemical Engineering, Low Dimensional Carbon Materials Center, Ulsan National Institute of Science and Technology (UNIST), Ulsan 689-798, South Korea

<sup>‡</sup>Department of Energy and Materials Engineering, Dongguk University, 26 Pil-dong, 3 ga, Jung-gu, Seoul 100-715, South Korea

<sup>§</sup>Pohang Accelerator Laboratory, Pohang University of Science and Technology, Pohang, Kyungbuk 790-784, South Korea

### Supporting Information

**ABSTRACT:** Structure–property relationships associated with a hybrid siloxane-terminated hexyl chain (SiC6), photophysics, molecular packing, thin-film morphology, and charge carrier transport are reported for two novel naphthalene diimide (NDI)-based polymers; P(NDI2SiC6-T2) consists of NDI and bithiophene (T2) repeating units, while for P(NDI2SiC6-TVVT), the (*E*)-2-(2-(thiophen-2-yl)-vinyl)thiophene (TVVT) units are introduced into the NDI-based backbone. The analysis of the optical spectra shows that the preaggregation of these polymers in solution is highly sensitive to the choice of solvent such that the films prepared by using different solvents can be “tuned” with regard to their degrees and types of the aggregates. In-depth morphology investigations (atomic force microscopy (AFM), grazing incidence X-ray diffraction (GIXD), and near-edge X-ray absorption fine structure (NEXAFS)) combined with device optimization studies are used to probe the interplay between molecular structure, molecular packing, and OFET mobility. It is found that the polymer films cast as a coating from chloroform (CF) solvent favor a mixed face-on and edge-on orientation, while 1-chloronaphthalene (CN)-cast films favor an almost entirely edge-on orientation, resulting in a difference in mobility between CF- and CN-cast devices. Within this work, the annealed P(NDI2SiC6-T2) device fabricated from CF, despite showing a less densely packed organization, shows the highest electron mobility of up to  $1.04 \text{ cm}^2/\text{V}\cdot\text{s}$  due to a highly balanced face-on to edge-on ratio. This work, for the first time, advances our understanding for how the balanced face-on to edge-on ratio plays a dramatic role in facilitating charge transport, opening a new charge-transport mechanism in electronic devices.



### INTRODUCTION

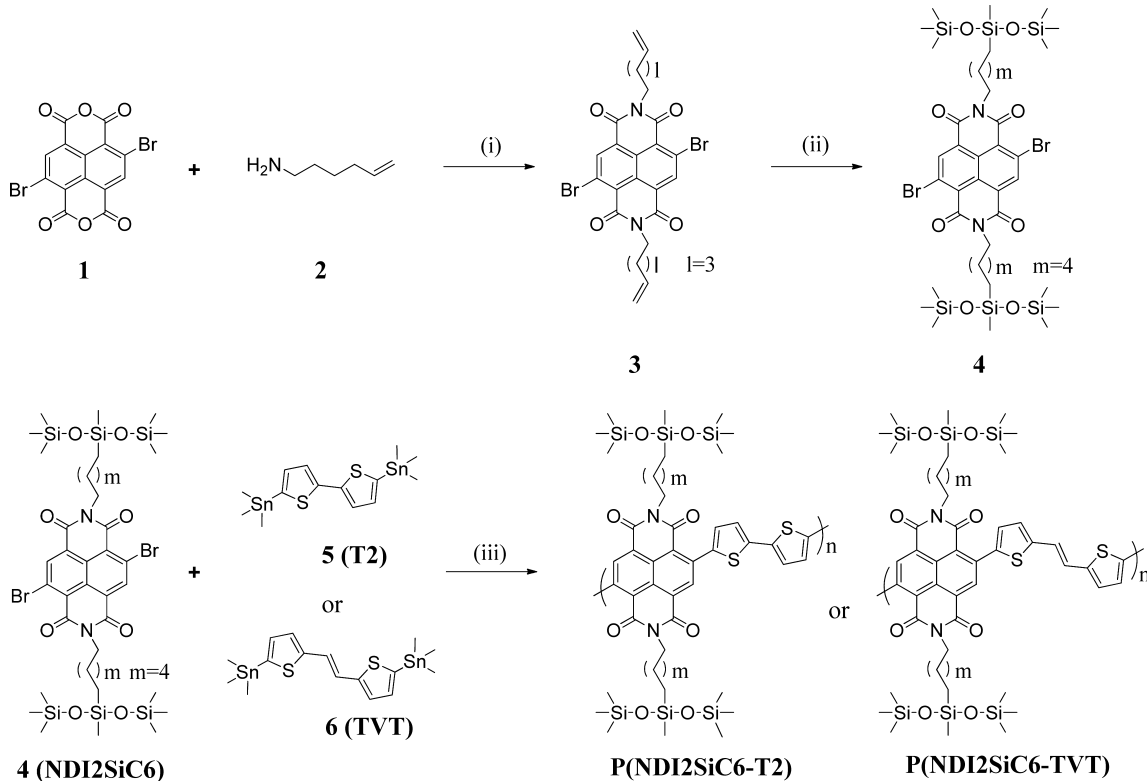
Significant efforts have been made toward the development of solution-processable polymeric materials for organic field-effect transistors (OFETs) because of their facile processability in solution at a relatively low temperature, which can open a new paradigm in application for flexible electronics and device manufacturing through cost-effective graphic art printing processes.<sup>1–9</sup> Current state-of-the-art polymers have been developed for use in p-channel OFETs with hole mobilities surpassing  $10 \text{ cm}^2/\text{V}\cdot\text{s}$ ;<sup>1,10–12</sup> however, the distinct lack of high-performance, ambient-stable, solution processed n-channel OFETs has hindered the development of low cost organic complementary circuits.<sup>13–23</sup> Therefore, not only is the development of reliable n-channel polymeric semiconductors a crucial issue but also a challenge for this type of polymers is a deep understanding and control of the layer morphology in organic electronics.

A breakthrough in n-channel polymers occurred with the development of P(NDI2OD-T2) polymer, containing naph-

thalene diimide (NDI) and bithiophene (T2) repeating units, by Facchetti and co-workers, demonstrating unprecedented OFET characteristics with electron mobility of up to  $0.85 \text{ cm}^2/\text{V}\cdot\text{s}$  in the device architecture.<sup>24,25</sup> Interestingly, P(NDI2OD-T2) thin films predominantly formed a dense in-plane molecular packing with only weak out-of-plane  $\pi$ -stacking order. Although the P(NDI2OD-T2) showed a best OFET characteristics with such face-on textures,<sup>26</sup> there were several attempts to achieve its out-of-plane ordering, which would be expected to exhibit better charge carrier mobility characteristics.<sup>27–29</sup> However, in previous reports, the out-of-plane ordered structures in P(NDI2OD-T2) that can be obtained by lowering surface energy via surface treatment and high-temperature thermal annealing reduced the electron mobility

Received: May 13, 2015

Revised: July 5, 2015

**Scheme 1.** Synthesis of P(NDI2SiC6-T2) and P(NDI2SiC6-TVT)<sup>a</sup>

<sup>a</sup>Reagents and conditions: (i) Acetic acid, 120 °C, 29% (ii) 1,1,1,3,5,5-heptamethyltrisiloxane, Karstedt catalyst ( $C_8H_{18}OPtSi_2$ , Pt 2% xylene solution), toluene, 90 °C, 26% (iii)  $Pd_2(dbu)_3$ ,  $P(o\text{-tolyl})_3$ , toluene, 110 °C, 48 h; P(NDI2SiC6-T2) (29%) and P(NDI2SiC6-TVT) (73%).

by an order of magnitude ( $10^{-2}$  cm<sup>2</sup>/V·s) from that of the pristine device.<sup>30</sup>

A more recent study by Fabiano and co-workers clearly indicated that the edge-on orientation of a few layers of P(NDI2OD-T2) derived from the Langmuir-Schäfer method shows the low electron mobility of  $\sim 10^{-3}$  cm<sup>2</sup>/V·s relative to that of the face-on orientation ( $\mu_{\text{electron}} = 0.1\text{--}0.5$  cm<sup>2</sup>/V·s).<sup>28,31</sup> These results challenge the traditional assumption that high carrier mobility is unambiguously linked to the high crystallinity morphology of the edge-on orientation for obtaining in-plane strong  $\pi\text{--}\pi$  stacking.<sup>29,32–36</sup> Very recently, the hindrance of the electron injection from the source/drain electrodes that is attributed to the vertically aligned long branched side chains (2-octyldodecyl solubilizing groups (2OD)) that have the same direction with the P(NDI2OD-T2) backbones is proposed as the main reason for the poor OFET characteristics in the edge-on oriented P(NDI2OD-T2) thin film.<sup>19</sup>

As a result, P(NDI2OD-T2) OFETs with preferential face-on orientation showed a relatively low  $R_c$  for electron injection due to a shorter hopping distance between the charge injection electrode and the frontier orbitals of P(NDI2OD-T2). In terms of this understanding, the best morphology to achieve both high mobility and low  $R_c$  in P(NDI2OD-T2) is a mixture of face-on orientation at the contact region and edge-on orientation in the channel region. Indeed, a remarkably improved electron mobility was reported for (*E*)-2-(2-(thiophen-2-yl)-vinyl)thiophene (TVT)-containing NDI polymer (P(NDI2OD-TVT)) that coexists with face-on and edge-on orientations.<sup>18,19</sup>

Apart from the molecular engineering of the conjugated backbones, recently, it was demonstrated that manipulating the

side chains has a big impact on molecular packing, film microstructure, and charge transport.<sup>2,3,37–39</sup> Although there is currently a relatively large side chain toolbox, systematic investigation on siloxane-terminated alkyl side chain-dependent molecular packing and OFET performance for NDI-based polymers is a fascinating topic because (i) the siloxane-terminated alkyl side chain is referred to as a hybrid organic/inorganic material in which the hybridization of organic and inorganic building blocks can combine their particular advantages; (ii) the previous investigations of the siloxane solubilizing groups are limited to the study of unipolar p-channel and p-channel dominant semiconductors;<sup>1–3,40</sup> studies on the critical role of siloxane-based hydrid side chains on charge transport properties for n-channel organic semiconductors are thus highly desired; and (iii) advancing our understanding of the multifunctional nature of hybrid side chains is essential for academic research and innovative industrial applications.

Herein, we describe the introduction of hybrid siloxane-terminated hexyl chains (SiC6) onto the NDI-T2 and NDI-TVT polymer backbones, to afford P(NDI2SiC6-T2) and P(NDI2SiC6-TVT), respectively (Scheme 1). By utilizing a combination of OFET characterizations, atomic force microscopy (AFM), grazing incidence X-ray diffraction (GIXD), and near-edge X-ray absorption fine structure (NEXAFS) spectroscopy, in-depth study on the siloxane-based side chain-dependent molecular packing and charge transport of P(NDI2SiC6-T2) and P(NDI2SiC6-TVT) is thoroughly carried out.

We discovered that for these polymers the polymer film-packing orientation can be controlled by changing the solvent

**Table 1.** Optical and Electrochemical Properties of P(NDI2SiC6-T2) and P(NDI2SiC6-TVT)

polymer	$M_n$ (kDa)/PDI <sup>a</sup>	$\lambda_{\max}$ soln (nm) room temp. <sup>b</sup>			elevated temp <sup>c</sup>		$\lambda_{\max}$ film (nm) <sup>d</sup>		$E_g^{\text{opt}}$ (eV) <sup>e</sup>	LUMO (eV) <sup>f</sup>	HOMO (eV) <sup>g</sup>
		CF	TCB	CN	TCB	CN	CF	CN			
P(NDI2SiC6-T2)	32/2.02	709	717	632	628	611	714	712	1.44	-3.83	-5.27
P(NDI2SiC6-TVT)	15/3.28	747	736	652	643	646	730	729	1.40	-3.96	-5.36

<sup>a</sup>GPC versus polystyrene standards in THF as eluent. <sup>b</sup>Solution absorption spectra at 25 °C. <sup>c</sup>Solution absorption spectra over 80 °C for TCB and CN as solvent. <sup>d</sup>Thin film absorption spectra from spin-cast from TCB and CN solution. <sup>e</sup>Optical energy gap estimated from the absorption onset of the thin films. <sup>f</sup>Cyclic voltammetry determined with Fc/Fc<sup>+</sup> as an internal reference (LUMO = -4.8 - ( $E_{1/2\text{red}}^{\text{first}} - E_{1/2\text{ox}}^{\text{Fc/Fc}^+}$ )) using thin film prepared with CF solution. <sup>g</sup>Estimated from HOMO = LUMO -  $E_g^{\text{opt}}$ .

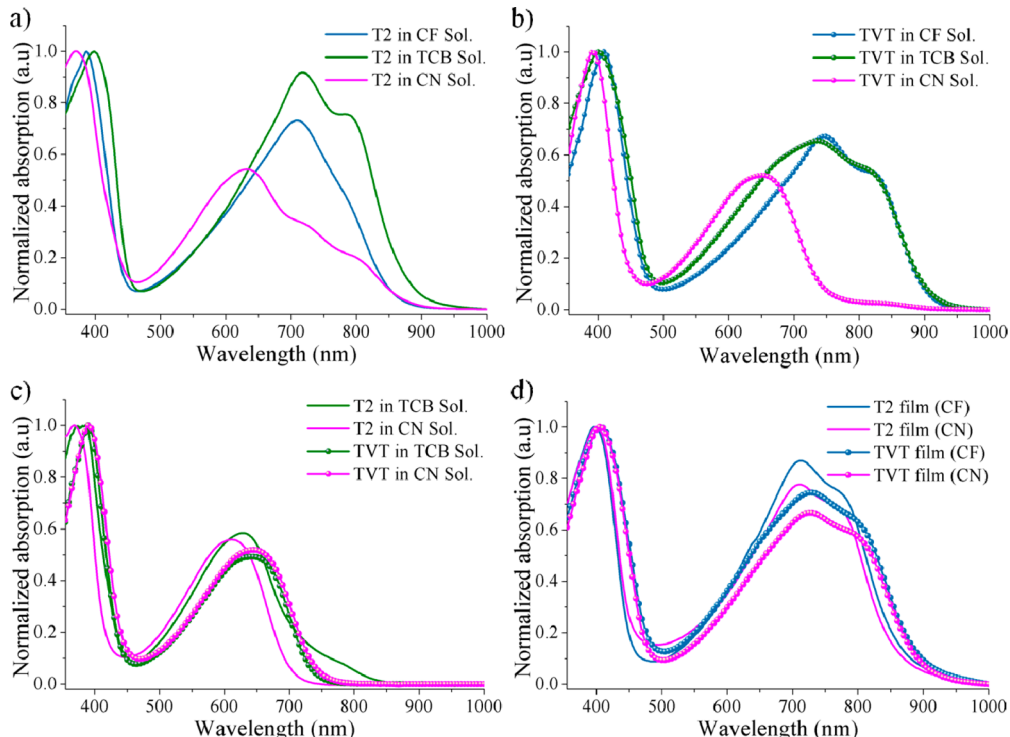


**Figure 1.** UV-vis absorption spectra of P(NDI2SiC6-T2) and P(NDI2SiC6-TVT) in (a) CF, TCB, and CN for P(NDI2SiC6-T2) at room temperature. (b) CF, TCB, and CN for P(NDI2SiC6-TVT) at room temperature. (c) TCB and CN over 80 °C for each polymer and (d) as thin solid films fabricated with CF and CN for each polymer.

used for the device fabrication; chloroform (CF)-cast films favored a mixed face-on and edge-on orientation, while 1-chloronaphthalene (CN)-cast films favored an almost entirely edge-on packing relative to the substrate. An exciting electron mobility greater than 1 cm<sup>2</sup>/V·s is observed for the annealed P(NDI2SiC6-T2) films fabricated from CF solvent, despite the relatively poor packing registry along both lamellar and  $\pi$ -stacking directions. This intriguing result is a clear indication of how the coexistence of face-on and edge-on orientations and a balanced face-on to edge-on ratio has a strong impact on the electron transport properties.

## RESULTS AND DISCUSSION

### Synthetic Strategies, Synthesis, and Characterization.

The synthetic routes to solution-processable polymers based on NDI consisting exclusively of SiC<sub>6</sub> solubilizing groups are outlined in **Scheme 1** and the detailed procedures and characterization data are described in the Experimental Section in **Supporting Information**. Briefly, *N,N'*-bis(hex-5-en-1-yl)-2,6-dibromonaphthalene-1,4,S,8-tetracarboxylic diimide (3) was

synthesized by condensation of 2,6-dibromonaphthalene-1,4,S,8-tetracarboxylic dianhydride (1) with 6-amino-1-hexene (2) that was obtained by Gabriel synthesis using 6-bromo-1-hexene and potassium phthalimide salt. Then, hydrosilylation of the terminal alkene with 1,1,1,3,S,5-heptamethyltrisiloxane was achieved in the presence of Karstedt catalyst, generating highly soluble NDI monomer (NDI2SiC<sub>6</sub>) with SiC<sub>6</sub> solubilizing chains. A Stille-coupling polymerization between bis-stannylated comonomers, T2 or TVT, and NDI2SiC<sub>6</sub> was employed to afford P(NDI2SiC<sub>6</sub>-T2) and P(NDI2SiC<sub>6</sub>-TVT). Both polymers were obtained as dark solids after careful purification by precipitation in methanol and subsequent Soxhlet extraction with methanol, acetone, hexane, and chloroform. Molecular weights of the polymers were determined by gel permeation chromatography (GPC), using polystyrene standards as calibrants with THF as eluent (**Table 1**). In contrast to the high solubility of P(NDI2SiC<sub>6</sub>-T2) in common organic solvents, P(NDI2SiC<sub>6</sub>-TVT) is less soluble in THF. Therefore, the reported GPC data only represent the soluble fractions of each sample in THF.

**Photophysical and Electrochemical Properties as well as Computational Studies.** It is well-known that optical properties of NDI-based materials can be widely tuned, for example, by changing solubilizing groups or solvents, due to the different types and degrees of their aggregation.<sup>17,41,42</sup> Thereby, to gain the detailed optical picture in our new class of polymers, we recorded the absorption spectra of P(NDI2SiC6-T2) and P(NDI2SiC6-TVT) both in solution and as thin films, by using different solvents, such as chloroform (CF), trichlorobenzene (TCB), and 1-chloronaphthalene (CN); the relevant data are collected in Table 1.

Both NDI-based polymers showed similar dual absorption bands in any solution and films: one broad absorption peak in the low-energy region (500–950 nm), corresponding to the strong charge transfer (CT) transition, and another one in the high-energy region (330–470 nm) arising from  $\pi-\pi^*$  transitions (see Figure 1). Both the solution and film spectra of P(NDI2SiC6-TVT) are red-shifted relative to those of P(NDI2SiC6-T2), which is commonly explained by the extended conjugation length as well as enhanced CT effects in TTV units.<sup>18,19</sup> Interestingly, both polymers show marked red-shifted absorptions in CF or TCB when compared to those in CN. In addition, the spectra of the polymer solutions at an elevated temperature (80 °C) exhibit a broad and featureless band centered at 632 nm for P(NDI2SiC6-T2) and 652 nm for P(NDI2SiC6-TVT), respectively, which is similar to the corresponding absorption profiles seen in each polymer in CN. Therefore, in both cases, this is solid evidence that the chain aggregation occurring in CN is apparently rather weak or even absent, while a preaggregated state prevails in the other solvents like CF and TCB. Additionally, a continuous decrease of the fraction of the polymers in the aggregated state can be induced by raising temperature.

Although the chromatic shifts of both polymer films spin-coated from CN are quite identical to the corresponding ones of the most structured spectra observed in CF, the intensities of the CT bands are somewhat increased when going from CN to CF. This indicates that both polymers show a pronounced tendency to aggregate during film formation, regardless of the solvents, but the aggregate content and type would be dependent on the chosen solvent. Optical band gaps ( $E_g^{\text{opt}}$ s), estimated from the absorption onset of polymer films, are listed in Table 1.

The electronic energy levels of both polymers were measured by cyclic voltammetry (CV) calibrated using a ferrocene/ferrocenium redox couple as an internal standard, showing only two reversible reduction waves within the solvent operating window (2 V) (see Supporting Information Figure S1). Thus, using their  $E_g^{\text{opt}}$ s and LUMO values, we calculated their HOMO levels and the data are summarized in Table 1. Notably, it was found that the replacement of T2 with TTV simultaneously changed the HOMO and LUMO levels of the polymer, resulting in a narrower bandgap in P(NDI2SiC6-TVT) with respect to that in P(NDI2SiC6-T2).

The optimized geometries and electron density distributions of the NDI-based trimers were calculated at B3LYP/6-31G\* level (Supporting Information Figure S2). The dihedral angles between thiophene and neighboring vinylene or thiophene units are  $\theta_{\text{T-Vinyl}} = 4.09^\circ$  and  $\theta_{\text{T-T}} = 3.92^\circ$ , respectively, and the angles between NDI and neighboring thiophene units are similar in both cases ( $\theta = 36.6$ – $37.4^\circ$ ). These values are similar to those of NDI-based polymers with common alkyl chains,<sup>18,43</sup> indicating that side chain engineering does not have a strong

impact on optimizing the geometry of NDI-based donor–acceptor polymers. This modeling study also suggests that the incorporation of vinyl groups into polymer backbones has a negligible influence on the dihedral angles between NDI and adjacent thiophene units. For both the model oligomers, the HOMOs show a high electron density around the thiophene units, whereas the LUMOs are localized on the NDI unit, similar to those of many other donor–acceptor polymers.

**Electrical Performance of OFETs.** We fabricated top-gate, bottom-contact (TG/BC) OFETs based on P(NDI2OD-T2), P(NDI2SiC6-T2), and P(NDI2SiC6-TVT). For the sake of comparison, P(NDI2OD-T2) was used as a reference polymer. The polymer thin films (20–22 nm) were prepared by spin-coating of the NDI polymer solutions in CF (4 mg/mL) in which the most enhanced solvent inducing preaggregation is shown and sequentially annealed at 100, 200, and 300 °C for 30 min in a nitrogen-filled glovebox.

Figure 2 shows typical transfer and output characteristics of P(NDI2SiC6-T2) and P(NDI2SiC6-TVT) OFETs. Both

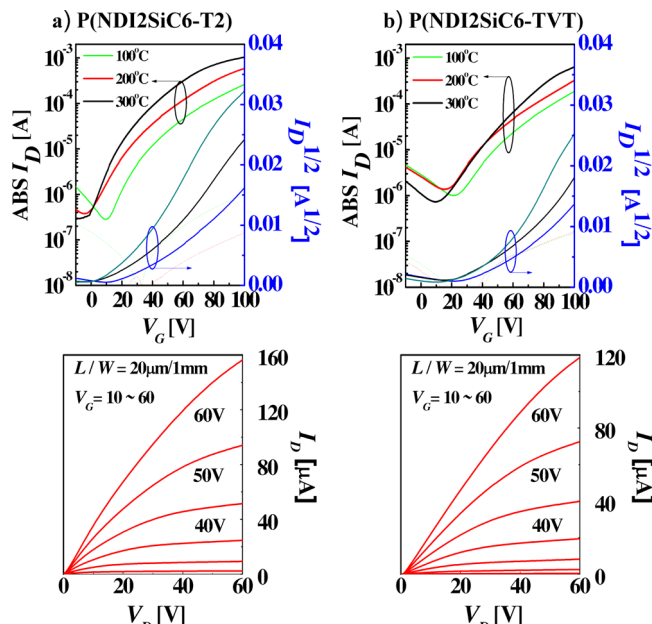


**Figure 2.** Current–voltage ( $I$ – $V$ ) characteristics of the OFETs fabricated with (a) P(NDI2SiC6-T2) and (b) P(NDI2SiC6-TVT) using CF as solvent and output characteristics of the devices annealed at 300 °C.

P(NDI2SiC6-T2) and P(NDI2SiC6-TVT) OFETs exhibited typical *n*-channel OFET characteristics and the electron mobilities of both devices were progressively improved by the increased annealing temperature. After annealing at 300 °C, the maximum mobility of the P(NDI2SiC6-T2) was determined to be as high as  $1.04 \text{ cm}^2/\text{V}\cdot\text{s}$ , which was slightly higher than that of P(NDI2SiC6-TVT) devices ( $\mu_{\text{elec}} = 0.93 \text{ cm}^2/\text{V}\cdot\text{s}$ ) (see Table 2). These exciting high mobilities are three times higher than that of the optimized reference polymer (P(NDI2OD-T2)) ( $\mu_{\text{elec}} = 0.32 \text{ cm}^2/\text{V}\cdot\text{s}$ , see Supporting Information Figure S3).

We note that the electron mobilities are much higher for both P(NDI2SiC6-T2) and P(NDI2SiC6-TVT) compared to P(NDI2OD-T2), despite the very similar LUMO energy levels, suggesting that other factors, such as molecular packing/crystallinity of the polymers can strongly influence their charge

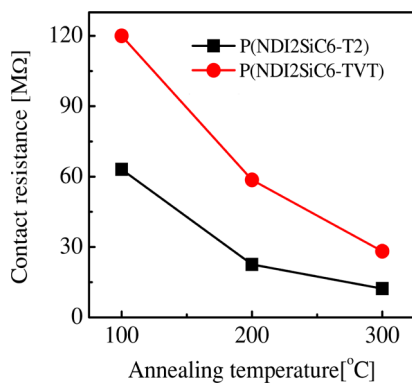
**Table 2.** Parameters of the TG/BC OFETs with Different Annealing Temperature

semiconductor <sup>a</sup>	annealing temp/time [°C/min]	$\mu_{e,\text{avg}}$ [cm <sup>2</sup> /V·s] <sup>b</sup>	V <sub>Th</sub> [V]	I <sub>on/off</sub>
P(NDI2SiC6-T2) (CF solvent)	100/30	0.43 ( $\pm 0.14$ )	25.1 ( $\pm 4.00$ )	10 <sup>3</sup>
	200/30	0.79 ( $\pm 0.25$ )	22.4 ( $\pm 3.50$ )	10 <sup>3</sup>
	300/30	1.04 ( $\pm 0.21$ )	21.6 ( $\pm 4.17$ )	10 <sup>3</sup>
P(NDI2SiC6-TVT) (CF solvent)	100/30	0.38 ( $\pm 0.11$ )	38.7 ( $\pm 4.00$ )	10 <sup>3</sup>
	200/30	0.62 ( $\pm 0.21$ )	36.4 ( $\pm 3.50$ )	10 <sup>3</sup>
	300/30	0.93 ( $\pm 0.20$ )	33.6 ( $\pm 4.17$ )	10 <sup>3</sup>
P(NDI2SiC6-T2) (CN solvent)	100/30	0.27 ( $\pm 0.32$ )	23.7 ( $\pm 3.80$ )	10 <sup>3</sup>
	200/30	0.48 ( $\pm 0.22$ )	23.3 ( $\pm 3.80$ )	10 <sup>3</sup>
	300/30	0.85 ( $\pm 0.23$ )	20.6 ( $\pm 4.70$ )	10 <sup>3</sup>
P(NDI2SiC6-TVT) (CN solvent)	100/30	0.33 ( $\pm 0.20$ )	25.6 ( $\pm 4.10$ )	10 <sup>3</sup>
	200/30	0.43 ( $\pm 0.20$ )	28.4 ( $\pm 4.10$ )	10 <sup>3</sup>
	300/30	0.78 ( $\pm 0.25$ )	31.6 ( $\pm 4.67$ )	10 <sup>3</sup>

<sup>a</sup>Semiconductor OFET devices fabricated by spin-coating onto Au S/D electrodes using CF and CN as solvent. <sup>b</sup>The average mobilities of the OFET devices were measured with  $L = 20 \mu\text{m}$ ,  $W = 1000 \mu\text{m}$ , and  $V_D = 100 \text{ V}$ . All electrical characteristics were obtained from the top-gate based transistors more than 20 devices.

transport properties. This idea will be discussed further in a subsequent thin-film morphology study.

The variation of FET mobilities is highly dependent on contact resistance. Thus, to evaluate contact effects we applied the Y-function method (YFM) described previously.<sup>44</sup> The detailed description of the specific analysis and equations employed are found in Experimental Section in Supporting Information. The YFM enables us to precisely obtain the  $R_c$  and low-field mobility ( $\mu_0$ ) from individual devices. The relevant data are listed in Supporting Information Table S1. In both OFETs, the  $R_c$  values were gradually reduced as a function of the increased temperature. At each temperature, P(NDI2SiC6-T2) OFETs showed lower  $R_c$  values than those of the corresponding P(NDI2SiC6-TVT) OFETs (Figure 3). These findings agree very well with the trends of the changed mobilities described above.

**Figure 3.** Contact resistance of the OFET devices upon different annealing temperatures.

Furthermore, we expanded the OFETs analyses to both P(NDI2SiC6-T2) and P(NDI2SiC6-TVT) films prepared from CN that mostly inhibits their preaggregations, because the dependence for each of the analyzed films was observed upon changing CF to CN, as already described in the previous section. As was observed for the OFETs fabricated from CF,

both polymer films formed when employing CN as solvent followed a similar tendency to increased mobilities with elevated annealing temperature over the range of 100 to 300 °C (Supporting Information Figure S4); P(NDI2SiC6-T2) ( $\mu_{\text{elec}} = 0.85 \text{ cm}^2/\text{V}\cdot\text{s}$ ) showed slightly higher electron mobility than that of P(NDI2SiC6-TVT) ( $\mu_{\text{elec}} = 0.78 \text{ cm}^2/\text{V}\cdot\text{s}$ ) (see Table 2). Obviously, it should be noted that the CF-cast films which show the microstructured absorption spectra revealed somewhat superior mobilities in general relative to the performances of the corresponding CN-cast OFET devices. These results corroborate that the film-packing orientations are influenced upon solvent selection (changing from CN to CF) because the molecular packing (degree of crystallinity and preference of ordering along the different crystallographic directions) strongly impacts the electronic coupling between molecules and the resulting charge carrier mobility.<sup>43,46</sup>

#### Thin-Film Morphology and Nanostructural Order.

First, information about the surface topography of the films fabricated from CF was gained with atomic force microscopy (AFM) images. As shown in Figure 4, although slightly coarsened domains can be observed in both samples annealed at 300 °C, thermal annealing has no obvious effect on the film topographies, and the typical fibril-like features of the as-spun layers are well preserved.

Furthermore, to determine the extent of cofacial π-stacking, crystallinity, and polymer-packing orientation relative to the substrate, we characterized the as-spun and annealed films at 300 °C for P(NDI2SiC6-T2) and P(NDI2SiC6-TVT) prepared from both CN and CF, respectively, by using grazing incidence X-ray diffraction (GIXD) measurement. These studies can allow access to the origin of the high electron mobility and the reasons why variations in deposition conditions, such as annealing and solvent, lead to different mobility values. Typical out-of-plane and in-plane diffraction curves and the detailed crystallographic parameters extracted from those GIXD patterns are shown in Figure 5 and Table 3, respectively.

Both as-spun P(NDI2SiC6-T2) and P(NDI2SiC6-TVT) films in CF exhibited well-defined multiple ( $h00$ ) diffraction patterns along the  $q_z$  (out-of-plane) axis corresponding to a highly ordered lamellar structure; (i) the observed lamellar  $d$ -spacing of P(NDI2SiC6-TVT) (27.6 Å) is similar to that of P(NDI2SiC6-T2) and (ii) a (010) diffraction peak arising from π-π stacking is clearly observed for P(NDI2SiC6-T2), while this peak is not found in P(NDI2SiC6-TVT).

When both the P(NDI2SiC6-T2) and P(NDI2SiC6-TVT) films were annealed at 300 °C, the peaks in the diffraction pattern became more defined and visible, suggesting the formation of more closed lamellar structures. For both annealed films coated from CF, two perpendicular features with  $\mathbf{q}$  vectors compatible with the (100) and (010) peaks obtained with GIXD can be observed, confirming the coexistence of face-on and edge-on orientations.

We are able to quantify the crystallite orientation distribution using an intensity-corrected pole figure plot along the (200) diffraction peaks described previously.<sup>1</sup> Briefly, for each pole figure (see Figure 5), the integrated intensity is as a function of along the arcs, where ( $-90^\circ$  to  $90^\circ$ ) is defined as the semicircular angle between the crystallite orientation and the surface normal.<sup>27</sup>

The near vertical-cut ( $\chi = 0^\circ$ ) and horizontal-cut ( $\chi = \pm 90^\circ$ ) are associated with the edge-on and face-on crystallites, respectively, where the area ratio of the two peaks ( $\chi = 0^\circ$ –

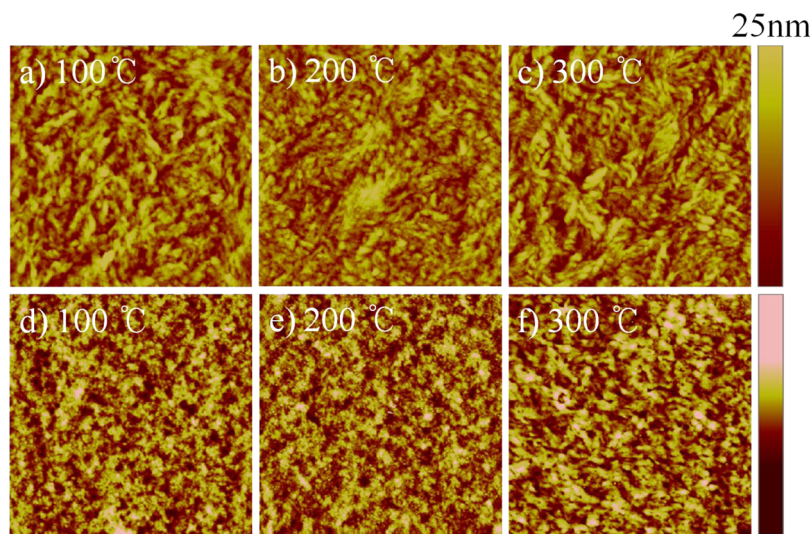


**Figure 4.** AFM height images of P(NDI2SiC6-T2) and P(NDI2SiC6-TVT) thin film prepared with CF at each annealed temperature. (a–c) Panels represent P(NDI2SiC6-T2) thin film; (d–f) panels represent P(NDI2SiC6-TVT) thin film ( $4 \times 4 \mu\text{m}$  size).

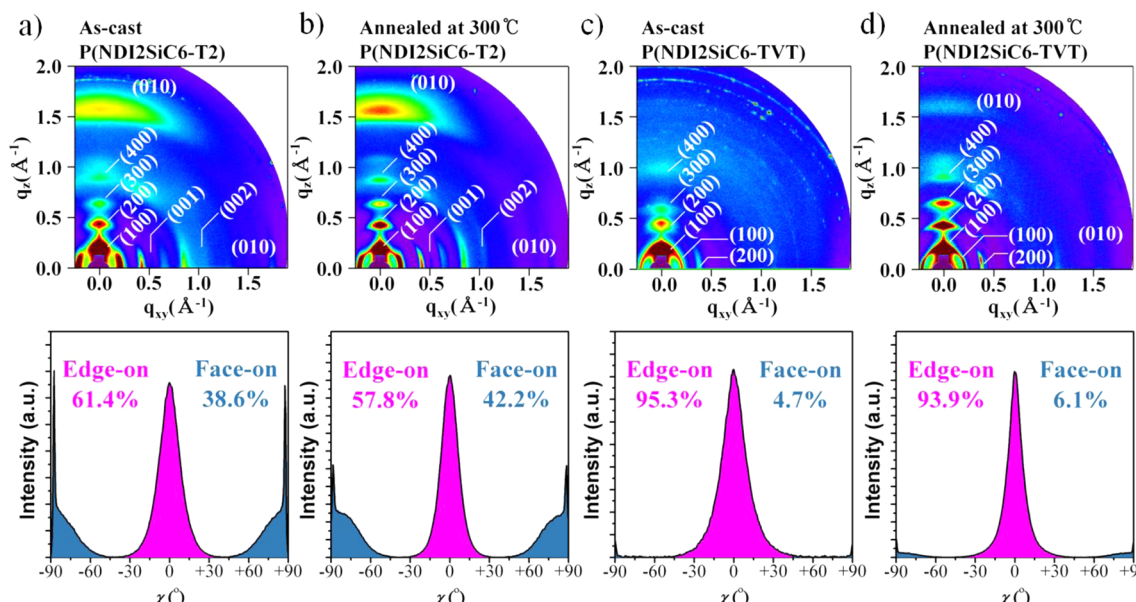


**Figure 5.** GIXD images and crystallite population of as-cast and annealed at 300 °C films fabricated by spin coating method using CF solution. (a,b) Panels represent thin film of P(NDI2SiC6-T2); (c,d) panels represent thin film of P(NDI2SiC6-TVT) under each condition.

$45^\circ$  and  $\chi = 45^\circ\text{--}90^\circ$ ) can be used to quantitatively access the portion of each crystallinity structure. The CF-pristine P(NDI2SiC6-T2) films show a clear bimodal distribution (edge-on (61.4%) versus face-on (38.6%)), whereas the CF-pristine P(NDI2SiC6-TVT) films have mainly edge-on structure (95.3%). In both cases, the thermal annealing slightly increases the face-on crystallite population (42.2% for P(NDI2SiC6-T2) and 6.1% for P(NDI2SiC6-TVT)) while maintaining their majority crystallite population and trend. These increases of face-on crystallite population after thermal annealing were estimated to be induced by the orientational preference of NDI-based polymers in cast film.<sup>17</sup>

Near-edge X-ray absorption fine structure (NEXAFS) spectroscopy provides information regarding the molecular orientation of the conjugated core complementary to GIXD. Therefore, the angle-dependent Carbon K-edge NEXAFS was performed on the as-cast and annealed (300 °C) films

fabricated using CF solution. Figure 6 shows the corresponding NEXAFS spectra collected in the incident X-ray angle range between 30° (~parallel to film surface) and 85° (~nominal to film surface). The lowest energy peaks appearing around 285 eV below the ionization step are associated with transitions from C-1s orbitals to  $\pi^*$  antibonding orbitals.<sup>35,47,48</sup> Because the resonance intensity of this transition is sensitive to the orientation of the transition dipole moment (TDM) with respect to the polarization of the incident X-ray beam, angular dependence of the intensity of these  $\pi^*$  resonances can be used to determine molecular orientation of the conjugated backbone. For example, if there is a strong angular dependence of the  $\pi^*$  resonance intensity with the largest value at normal incident angle (90°) to the film surface, this indicates that the conjugated plane is highly oriented and tilts away from the substrate in an edge-on orientation. However, all of the spectra show little angular dependence of the  $\pi^*$  resonance intensity, as

**Table 3. Crystallographic Parameters Calculated from GIXD Profiles**

preparation condition	crystallographic parameters	P(NDI2SiC6-T2)	P(NDI2SiC6-TVT)
as-cast CF (solvent)	(100) $q (\text{\AA}^{-1})$	0.213	0.228
	$d$ -spacing ( $\text{\AA}$ )	29.5	27.6
	$\pi-\pi$ $q (\text{\AA}^{-1})$	1.603	N/D <sup>a</sup>
		3.92	N/A <sup>b</sup>
annealing at 300 °C CF (solvent)	(100) $q (\text{\AA}^{-1})$	0.223	0.232
	$d$ -spacing ( $\text{\AA}$ )	28.2	27.1
	$\pi-\pi$ $q (\text{\AA}^{-1})$	1.62	1.63
		3.88	3.85
as-cast CN (solvent)	(100) $q (\text{\AA}^{-1})$	0.233	0.202
	$d$ -spacing ( $\text{\AA}$ )	27.0	31.1
	$\pi-\pi$ $q (\text{\AA}^{-1})$	N/D <sup>a</sup>	N/D
		N/A <sup>b</sup>	N/A
annealing at 300 °C CN (solvent)	(100) $q (\text{\AA}^{-1})$	0.228	0.199
	$d$ -spacing ( $\text{\AA}$ )	27.6	31.6
	$\pi-\pi$ $q (\text{\AA}^{-1})$	N/D	N/D
		N/A	N/A

<sup>a</sup>Any discernible  $\pi-\pi$  stack peak was not detected in as-cast thin film.

<sup>b</sup>The  $d$ -spacings could not be calculated due to the absence of  $\pi-\pi$  stack peak in as-cast thin film.

shown in the insets of Figure 6. The lack of strong angular dependence in the  $\pi^*$  resonance could be associated either with a well-balanced face-on to edge-on ratio as proved by our GIXD results. Thermal annealing of the as-cast films leads to the slightly increased peak intensities at high incident angles (i.e., nominal to substrate).

We expanded the GIXD analysis to films prepared from CN. All CN-cast polymer films show a similar diffraction pattern regardless of the thermal treatment; although it is possible to discern the presence of faint (h00) diffraction peaks in the out-of-plane, being assignable to lamellar stacking oriented randomly with respect to the substrate, the (010) diffraction peaks are not seen both in the  $q_z$  and  $q_{xy}$  vectors (see Figure 7 and Table 3). This suggests that the CN-cast films before and after annealing possess a rather amorphous microstructure with almost exclusively edge-on population, substantiating the results obtained from the optical spectra above; the CN-cast films showed the less structured absorption spectra than those of CF-cast films.

By incorporating GIXD and NEXAFS results with the device performances, and although the influence of molecular weight and PDI is not considered, we propose that the charge transport in NDI-based polymers correlates strongly not only with the coexistence of face-on with edge-on crystalline domains but also with the balanced face-on to edge-on ratios in NDI-based polymers. However, the  $\pi-\pi$  stacking distance and the packing conformation can directly affect the interpolymer chain carrier transport.<sup>17</sup> This finding is extremely significant because previous studies of polymer-packing orientation have mainly focused on how to adopt the

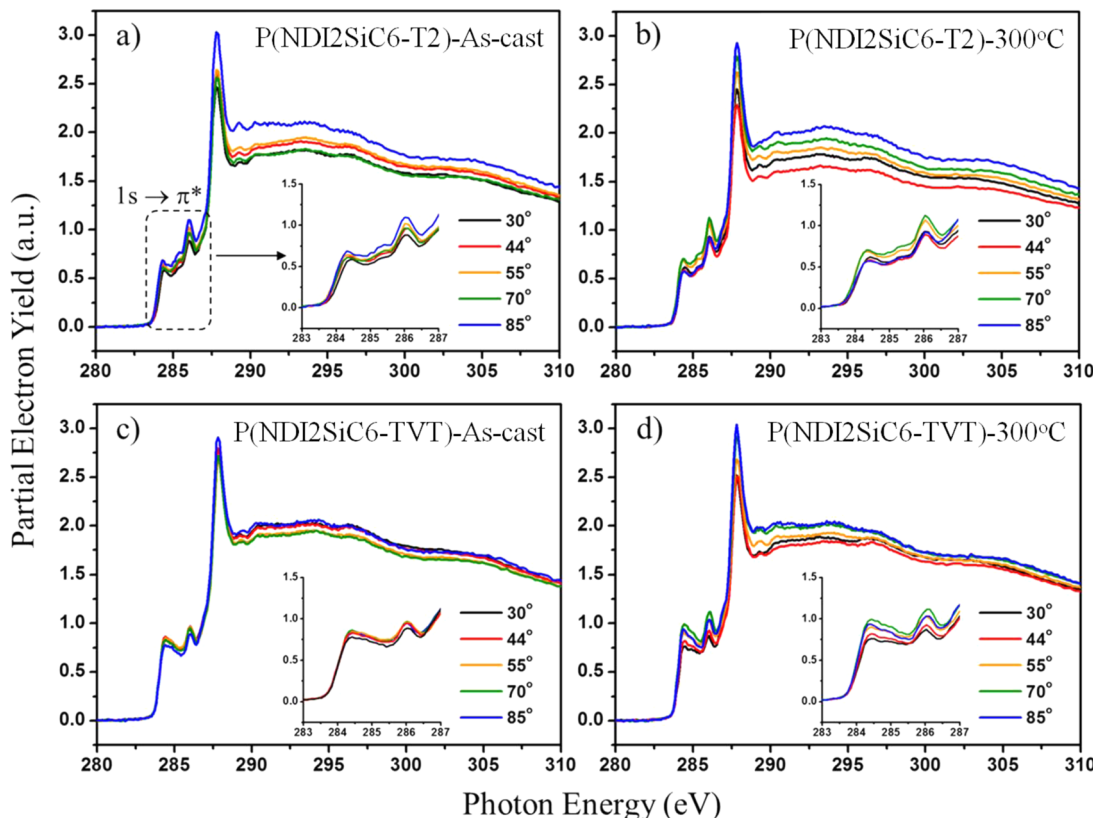


**Figure 6.** Angle-dependent carbon K-edge NEXAFS spectra of as-cast and annealed at 300 °C films fabricated by spin coating method using CF solution. (a,b) Panels represent thin film of P(NDI2SiC6-T2); (c,d) panels represent thin film of P(NDI2SiC6-TVT) under each condition. Insets show the magnified region of peaks corresponding to the resonant transitions of  $1s \rightarrow \pi^*$  antibonding orbitals.

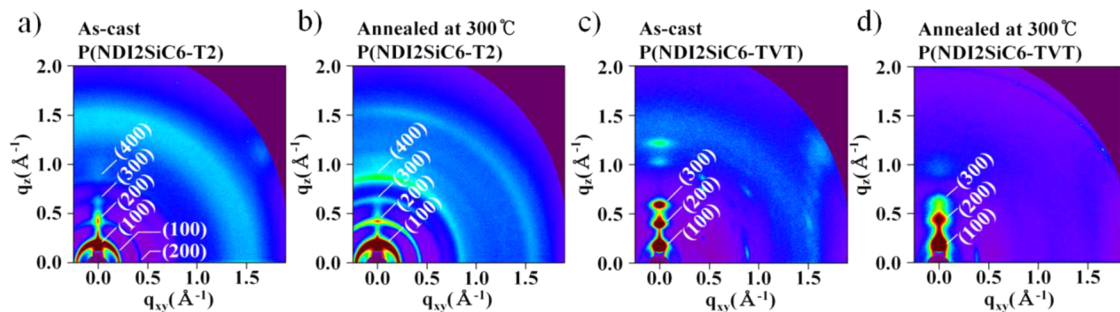


**Figure 7.** GIXD images of as-cast and annealed at 300 °C films fabricated by spin coating method using CN solution. (a,b) Panels represent thin film of P(NDI2SiC6-T2); (c,d) panels represent thin film of P(NDI2SiC6-TVT) under each condition.

preferential orientation order and the denser packing by tailoring structures and fabrication processing, and not on how to create the balanced mixture stacking structures with face-on and edge-on oriented molecules.

## CONCLUSION

With taking into account the cooperative properties and synergistic effects derived from hybridization of organic and inorganic species, a hybrid siloxane-terminated hexyl chain (SiC6) has been incorporated onto the NDI-based backbone to generate P(NDI2SiC6-T2) and P(NDI2SiC6-TVT), respectively. We have shown distinct changes in the optical absorptions of these two polymers in solution when varying the organic solvent. Among the tested solvents, in both polymer cases the most structured and red-shifted spectra are measured in CF, while the chain preaggregations in CN are almost absent. The intensities of the CT bands of the polymer films spin-coated from CF and CN solvents are slightly different, meaning that their aggregate content and type would be dependent on the chosen solvent. A combination of detailed electrical measurements by using OFET characterization and thin-film morphology studies (AFM, GIXD, and NEXAFS) reveals that the nature of the CF- and CN-cast films of each polymer has a significant influence on film morphology and molecular packing, thus affecting the charge transport properties. Regardless of the annealing treatment, P(NDI2SiC6-T2) and P(NDI2SiC6-TVT) devices fabricated from CF solvent show a mixed face-on and edge-on orientation, and edge-on orientation, respectively, whereas the corresponding CN-cast films exhibit a rather amorphous microstructure with almost exclusively edge-on population, indicating the significant role of the chosen solvent on molecular assembly properties for NDI-based polymers. The coexistence of face-on and edge-on orientations in the CF-cast films is responsible for their higher electron transport mobilities than those of the corresponding CN-cast films. In particular, the annealed P(NDI2SiC6-T2) films from CF, despite showing less packed ordering along both the lamellar and  $\pi$ -stacking directions, have a highly balanced face-on to edge-on ratio (42.2%:57.8%), resulting in the best electron mobility of up to 1.04 cm<sup>2</sup>/V·s. When the data from our current study are considered, for the first time, it is evident that the balanced face-on to edge-on ratio rather than the preferential orientation order especially for the polymer having NDI-T2 structure as its repeating unit and the strong  $\pi$ -stacking is a critical factor that governs charge transport, which provides a new test bench for the charge-transport mechanism.

## ASSOCIATED CONTENT

### Supporting Information

Cyclic voltammograms as well as calculated molecular orbitals for the model trimers of NDI-based polymers and current–voltage (*I*–*V*) characteristics of OFETs as well as contact resistance of TG/BC OFETs. The Supporting Information is available free of charge on the ACS Publications website at DOI: 10.1021/acs.macromol.5b01012.

## AUTHOR INFORMATION

### Corresponding Authors

\*E-mail: yynoh@dongguk.edu.

\*E-mail: yang@unist.ac.kr.

### Author Contributions

Y.K. and D.X.L. contributed equally.

### Notes

The authors declare no competing financial interest.

## ACKNOWLEDGMENTS

This work was supported by a National Research Foundation of Korea (NRF) grant (2013R1A1A1A05004475, 2010-0019408, BK21 Plus (10Z20130011057)), funded by the Korean Government (MSIP) (NRF-2014R1A2A2A01007159) and the 2014 Dongguk University Research Fund. Experiments at the PLS-II 9A U-SAXS beamline were supported, in part, by MEST and POSTECH. K.N. gratefully acknowledges the NSLS's U7A beamline scientists, Dr. Cherno Jaya and Dr. Daniel A. Fisher for their technical support.

## REFERENCES

- (1) Kim, G.; Kang, S.-J.; Dutta, G. K.; Han, Y.-K.; Shin, T. J.; Noh, Y.-Y.; Yang, C. *J. Am. Chem. Soc.* **2014**, *136*, 9477.
- (2) Lee, J.; Han, A.-R.; Kim, J.; Kim, Y.; Oh, J. H.; Yang, C. *J. Am. Chem. Soc.* **2012**, *134*, 20713.
- (3) Lee, J.; Han, A.-R.; Yu, H.; Shin, T. J.; Yang, C.; Oh, J. H. *J. Am. Chem. Soc.* **2013**, *135*, 9540.
- (4) Baeg, K.-J.; Caironi, M.; Noh, Y.-Y. *Adv. Mater.* **2013**, *25*, 4210.
- (5) Olivier, Y.; Niedzialek, D.; Lemaur, V.; Pisula, W.; Müllen, K.; Koldemir, U.; Reynolds, J. R.; Lazzaroni, R.; Cornil, J.; Beljonne, D. *Adv. Mater.* **2014**, *26*, 2119.
- (6) Henson, Z. B.; Mullen, K.; Bazan, G. C. *Nat. Chem.* **2012**, *4*, 699.
- (7) Tsao, H. N.; Cho, D. M.; Park, I.; Hansen, M. R.; Mavrinskiy, A.; Yoon, D. Y.; Graf, R.; Pisula, W.; Spiess, H. W.; Müllen, K. *J. Am. Chem. Soc.* **2011**, *133*, 2605.
- (8) Sirringhaus, H. *Adv. Mater.* **2014**, *26*, 1319.
- (9) Mei, J.; Diao, Y.; Appleton, A. L.; Fang, L.; Bao, Z. *J. Am. Chem. Soc.* **2013**, *135*, 6724.
- (10) Tseng, H.-R.; Phan, H.; Luo, C.; Wang, M.; Perez, L. A.; Patel, S. N.; Ying, L.; Kramer, E. J.; Nguyen, T.-Q.; Bazan, G. C.; Heeger, A. J. *Adv. Mater.* **2014**, *26*, 2993.

- (11) Li, J.; Zhao, Y.; Tan, H. S.; Guo, Y.; Di, C.-A.; Yu, G.; Liu, Y.; Lin, M.; Lim, S. H.; Zhou, Y.; Su, H.; Ong, B. S. *Sci. Rep.* **2012**, *2*, 754.
- (12) Kang, I.; Yun, H.-J.; Chung, D. S.; Kwon, S.-K.; Kim, Y.-H. *J. Am. Chem. Soc.* **2013**, *135*, 14896.
- (13) Newman, C. R.; Frisbie, C. D.; da Silva Filho, D. A.; Brédas, J.-L.; Ewbank, P. C.; Mann, K. R. *Chem. Mater.* **2004**, *16*, 4436.
- (14) Chua, L.-L.; Zaumseil, J.; Chang, J.-F.; Ou, E. C. W.; Ho, P. K. H.; Sirringhaus, H.; Friend, R. H. *Nature* **2005**, *434*, 194.
- (15) Oh, J. H.; Lee, H. W.; Mannsfeld, S.; Stoltzenberg, R. M.; Jung, E.; Jin, Y. W.; Kim, J. M.; Yoo, J.-B.; Bao, Z. *Proc. Natl. Acad. Sci. U. S. A.* **2009**, *106*, 6065.
- (16) Usta, H.; Risko, C.; Wang, Z.; Huang, H.; Deliomeroglu, M. K.; Zhukhovitskiy, A.; Facchetti, A.; Marks, T. J. *J. Am. Chem. Soc.* **2009**, *131*, 5586.
- (17) Steyrleuthner, R.; Di Pietro, R.; Collins, B. A.; Polzer, F.; Himmelberger, S.; Schubert, M.; Chen, Z.; Zhang, S.; Salleo, A.; Ade, H.; Facchetti, A.; Neher, D. *J. Am. Chem. Soc.* **2014**, *136*, 4245.
- (18) Chen, H.; Guo, Y.; Mao, Z.; Yu, G.; Huang, J.; Zhao, Y.; Liu, Y. *Chem. Mater.* **2013**, *25*, 3589.
- (19) Kim, R.; Amegadze, P. S. K.; Kang, I.; Yun, H.-J.; Noh, Y.-Y.; Kwon, S.-K.; Kim, Y.-H. *Adv. Funct. Mater.* **2013**, *23*, 5719.
- (20) Anthony, J. E.; Facchetti, A.; Heeney, M.; Marder, S. R.; Zhan, X. *Adv. Mater.* **2010**, *22*, 3876.
- (21) Sun, B.; Hong, W.; Yan, Z.; Aziz, H.; Li, Y. *Adv. Mater.* **2014**, *26*, 2636.
- (22) Sonar, P.; Singh, S. P.; Li, Y.; Soh, M. S.; Dodabalapur, A. *Adv. Mater.* **2010**, *22*, 5409.
- (23) Di Pietro, R.; Fazzi, D.; Kehoe, T. B.; Sirringhaus, H. *J. Am. Chem. Soc.* **2012**, *134*, 14877.
- (24) Yan, H.; Chen, Z.; Zheng, Y.; Newman, C.; Quinn, J. R.; Dötz, F.; Kastler, M.; Facchetti, A. *Nature* **2009**, *457*, 679.
- (25) Chen, Z.; Zheng, Y.; Yan, H.; Facchetti, A. *J. Am. Chem. Soc.* **2009**, *131*, 8.
- (26) Rivnay, J.; Toney, M. F.; Zheng, Y.; Kauvar, I. V.; Chen, Z.; Wagner, V.; Facchetti, A.; Salleo, A. *Adv. Mater.* **2010**, *22*, 4359.
- (27) Rivnay, J.; Steyrleuthner, R.; Jimison, L. H.; Casadei, A.; Chen, Z.; Toney, M. F.; Facchetti, A.; Neher, D.; Salleo, A. *Macromolecules* **2011**, *44*, 5246.
- (28) Fabiano, S.; Musumeci, C.; Chen, Z.; Scandurra, A.; Wang, H.; Loo, Y.-L.; Facchetti, A.; Pignataro, B. *Adv. Mater.* **2012**, *24*, 951.
- (29) Caironi, M.; Bird, M.; Fazzi, D.; Chen, Z.; Di Pietro, R.; Newman, C.; Facchetti, A.; Sirringhaus, H. *Adv. Funct. Mater.* **2011**, *21*, 3371.
- (30) Fabiano, S.; Yoshida, H.; Chen, Z.; Facchetti, A.; Loi, M. A. *ACS Appl. Mater. Interfaces* **2013**, *5*, 4417.
- (31) Cheng, X.; Noh, Y.-Y.; Wang, J.; Tello, M.; Frisch, J.; Blum, R.-P.; Vollmer, A.; Rabe, J. P.; Koch, N.; Sirringhaus, H. *Adv. Funct. Mater.* **2009**, *19*, 2407.
- (32) Sirringhaus, H.; Brown, P. J.; Friend, R. H.; Nielsen, M. M.; Bechgaard, K.; Langeveld-Voss, B. M. W.; Spiering, A. J. H.; Janssen, R. A. J.; Meijer, E. W.; Herwig, P.; de Leeuw, D. M. *Nature* **1999**, *401*, 685.
- (33) Chabinyc, M. L.; Toney, M. F.; Kline, R. J.; McCulloch, I.; Heeney, M. *J. Am. Chem. Soc.* **2007**, *129*, 3226.
- (34) Jimison, L. H.; Salleo, A.; Chabinyc, M. L.; Bernstein, D. P.; Toney, M. F. *Phys. Rev. B: Condens. Matter Mater. Phys.* **2008**, *78*, 125319.
- (35) Schuettfort, T.; Thomsen, L.; McNeill, C. R. *J. Am. Chem. Soc.* **2013**, *135*, 1092.
- (36) Li, Y.; Sonar, P.; Singh, S. P.; Soh, M. S.; van Meurs, M.; Tan, J. *J. Am. Chem. Soc.* **2011**, *133*, 2198.
- (37) Zhang, F.; Hu, Y.; Schuettfort, T.; Di, C.-a.; Gao, X.; McNeill, C. R.; Thomsen, L.; Mannsfeld, S. C. B.; Yuan, W.; Sirringhaus, H.; Zhu, D. *J. Am. Chem. Soc.* **2013**, *135*, 2338.
- (38) Lei, T.; Dou, J.-H.; Pei, J. *Adv. Mater.* **2012**, *24*, 6457.
- (39) Ha, Y.-g.; Emery, J. D.; Bedzyk, M. J.; Usta, H.; Facchetti, A.; Marks, T. J. *J. Am. Chem. Soc.* **2011**, *133*, 10239.
- (40) Mei, J.; Kim, D. H.; Ayzner, A. L.; Toney, M. F.; Bao, Z. *J. Am. Chem. Soc.* **2011**, *133*, 20130.
- (41) Steyrleuthner, R.; Schubert, M.; Howard, I.; Klaumünzer, B.; Schilling, K.; Chen, Z.; Saalfrank, P.; Laquai, F.; Facchetti, A.; Neher, D. *J. Am. Chem. Soc.* **2012**, *134*, 18303.
- (42) Schubert, M.; Dolfen, D.; Frisch, J.; Roland, S.; Steyrleuthner, R.; Stiller, B.; Chen, Z.; Scherf, U.; Koch, N.; Facchetti, A.; Neher, D. *Adv. Energy Mater.* **2012**, *2*, 369.
- (43) Giussani, E.; Fazzi, D.; Brambilla, L.; Caironi, M.; Castiglioni, C. *Macromolecules* **2013**, *46*, 2658.
- (44) Baeg, K.-J.; Bae, G.-T.; Noh, Y.-Y. *ACS Appl. Mater. Interfaces* **2013**, *5*, 5804.
- (45) Coropceanu, V.; Cornil, J.; da Silva Filho, D. A.; Olivier, Y.; Silbey, R.; Brédas, J.-L. *Chem. Rev.* **2007**, *107*, 926.
- (46) Brédas, J.-L.; Cornil, J.; Beljonne, D.; dos Santos, D. A.; Shuai, Z. *Acc. Chem. Res.* **1999**, *32*, 267.
- (47) Gann, E.; McNeill, C. R.; Szumilo, M.; Sirringhaus, H.; Sommer, M.; Maniam, S.; Langford, S. J.; Thomsen, L. *J. Chem. Phys.* **2014**, *140*, 164710.
- (48) Rivnay, J.; Noriega, R.; Northrup, J. E.; Kline, R. J.; Toney, M. F.; Salleo, A. *Phys. Rev. B: Condens. Matter Mater. Phys.* **2011**, *83*, 121306.